Immature truncated O-glycophenotype of cancer directly induces oncogenic features

Prakash Radhakrishnan[a,1], Sally Dabelsteen[b,c,1], Frey Brus Madsen[b,c], Chiara Francavilla[d], Katharina L. Kopp[b], Catharina Steentoft[b], Sergey Y. Vakhrushev[b], Jesper V. Olsen[d], Lars Hansen[b], Eric P. Bennett[b], Anders Woetmann[e], Guangliang Yin[f], Longyun Chen[f], Haiyan Song[f], Mads Bak[b], Ryan A. Hlady[a], Staci L. Peters[a], Rene Opavsky[a], Christenze Thode[c], Klaus Qvortrup[g], Katrine T.-B. G. Schjoldager[b], Henrik Clausen[b], Michael A. Hollingsworth[a], and Hans H. Wandall[b,2]

[a]Eppley Institute for Research in Cancer, Fred and Pamela Buffet Cancer Center, University of Nebraska Medical Center, Omaha, NE 68198-5950; [b]Copenhagen Center for Glycomics, Department of Cellular and Molecular Medicine, [c]Department of Pathology and Medicine, School of Dentistry, [d]Protein Center, [g]Department of Biomedical Sciences/Core Facility for Integrated Microscopy, and [e]Department of Immunology, Faculty of Health Sciences, University of Copenhagen, DK-2200 Copenhagen N, Denmark; and [f]BGI-Tech, BGI-Shenzhen, Shenzhen 518083, China

Edited by Stuart A. Kornfeld, Washington University School of Medicine, St. Louis, MO, and approved July 21, 2014 (received for review April 11, 2014)

Aberrant expression of immature truncated O-glycans is a characteristic feature observed on virtually all epithelial cancer cells, and a very high frequency is observed in early epithelial premalignant lesions that precede the development of adenocarcinomas. Expression of the truncated O-glycan structures Tn and sialyl-Tn is strongly associated with poor prognosis and overall low survival. The genetic and biosynthetic mechanisms leading to accumulation of truncated O-glycans are not fully understood and include mutation or dysregulation of glycosyltransferases involved in elongation of O-glycans, as well as relocation of glycosyltransferases controlling initiation of O-glycosylation from Golgi to endoplasmic reticulum. Truncated O-glycans have been proposed to play functional roles for cancer-cell invasiveness, but our understanding of the biological functions of aberrant glycosylation in cancer is still highly limited. Here, we used exome sequencing of most glycosyltransferases in a large series of primary and metastatic pancreatic cancers to rule out somatic mutations as a cause of expression of truncated O-glycans. Instead, we found hypermethylation of core 1 β3-Gal-T-specific molecular chaperone, a key chaperone for O-glycan elongation, as the most prevalent cause. We next used gene editing to produce isogenic cell systems with and without homogenous truncated O-glycans that enabled, to our knowledge, the first polyomic and side-by-side evaluation of the cancer O-glycophenotype in an organotypic tissue model and in xenografts. The results strongly suggest that truncation of O-glycans directly induces oncogenic features of cell growth and invasion. The study provides support for targeting cancer-specific truncated O-glycans with immunotherapeutic measures.

epigenetics | glycans | skin | pancreas | keratinocyte

Neoplastic transformation of human cells is virtually always associated with aberrant glycosylation of proteins and lipids (1), and the most frequently observed aberrant glycophenotype is expression of the most immature truncated O-glycan structures designated Tn and STn (Fig. 1*A*) (2–4). Truncated O-glycans are observed on virtually all epithelial cancer cells and many early epithelial premalignant lesions that precede the development of adenocarcinomas (3, 5–7). Expression of truncated O-glycans is strongly correlated with poor prognosis and low overall survival (2) and truncated O-glycans serve as targets for immunotherapies (4, 8). In addition O-glycopeptide epitopes composed of a truncated O-glycan and a short peptide sequence are emerging as true cancer-specific antigens targetable by drug-loaded antibodies and T cell-engaging immunotherapies (4, 9, 10). We have, however, a limited understanding of the molecular mechanisms leading to expression of truncated O-glycans in human tumors, as well as little understanding of the potential biological roles of truncating O-glycosylation in carcinogenesis (11).

Glycosylation of proteins is governed by ∼200 glycosyltransferases that reside in the secretory pathway and that, in a nontemplate fashion, orchestrate the diversity of glycan structures found on cells in a surprisingly well-defined manner (12). Mucin-type (GalNAc-type) O-glycosylation of proteins is an abundant and diverse form of posttranslational modification that is initiated by a family of up to 20 polypeptide GalNAc-transferases that decorate proteins with GalNAc residues (GalNAcα1-O-Ser/Thr; Tn antigen), which are further elongated, branched, and capped by a large number of different glycosyltransferases in subsequent processing steps (Fig. 1*A*). In normal cells, O-glycosylation proceeds to mature elongated and often branched O-glycans frequently capped by sialic acids (12). In contrast, cancer cells express only the early biosynthetic intermediates (4). The most common first elongation step is the core 1 O-glycan structure (Galβ1–3GalNAcα1-O-Ser/Thr; T antigen) and this step is catalyzed by a single enzyme, C1GalT1, that unusually requires a private chaperone, core 1 β3-Gal-T-specific molecular chaperone (*COSMC*), for folding and activity (13–16). The expression of the immature truncated Tn and STn O-glycans in cancers has been proposed to result from a number of different

Significance

Cancer cells characteristically express proteins with immature O-glycosylation, but how and why cancer cells express immature O-glycans has remained poorly understood. Here, we report that one prevalent mechanism in pancreatic cancer is epigenetic silencing, rather than somatic mutations in a key chaperone, core 1 β3-Gal-T-specific molecular chaperone (*COSMC*), required for mature elongated O-glycosylation. We also demonstrate, with the use of well-defined cell systems generated by precise gene editing, that the aberrant O-glycophenotype by itself induces oncogenic features with enhanced growth and invasion. Our study suggests that the characteristic aberrant O-glycophenotype is critical for the development and behavior of cancer and further provides support for immunotherapeutic strategies that target aberrant O-glycans.

Author contributions: P.R., S.D., F.B.M., C.F., K.L.K., C.S., J.V.O., L.H., E.P.B., G.Y., L.C., H.S., R.A.H., S.L.P., R.O., C.T., K.Q., K.T.-B.G.S., and H.H.W. designed research; P.R., S.D., F.B.M., C.F., K.L.K., C.S., S.Y.V., L.H., E.P.B., A.W., G.Y., L.C., H.S., M.B., R.A.H., S.L.P., R.O., C.T., K.Q., K.T.-B.G.S., and H.H.W. performed research; H.C. contributed new reagents/analytic tools; P.R., S.D., H.C., M.A.H., and H.H.W. analyzed data; and P.R., S.D., H.C., M.A.H., and H.H.W. wrote the paper.

The authors declare no conflict of interest.

This article is a PNAS Direct Submission.

Freely available online through the PNAS open access option.

See Commentary on page 14009.

[1]P.R. and S.D. contributed equally to this work.

[2]To whom correspondence should be addressed. Email: hhw@sund.ku.dk.

This article contains supporting information online at www.pnas.org/lookup/suppl/doi:10.1073/pnas.1406619111/-/DCSupplemental.

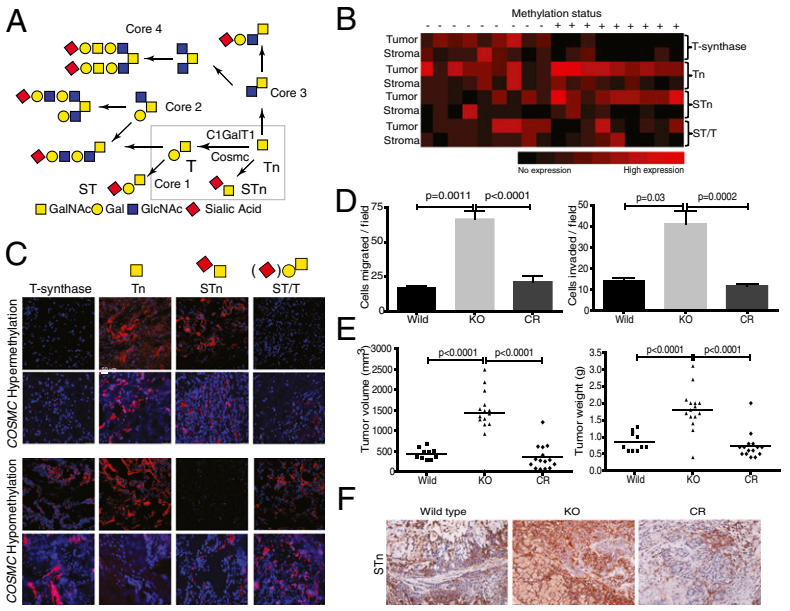

Fig. 1. Truncated O-glycans affect the biology of human pancreatic cancer. (*A*) Depiction of common biosynthetic pathways of mucin-type O-glycans illustrating truncated O-glycan structures associated with cancer (boxed) and the key regulatory role the core 1 synthase (C1GalT1) and its private chaperone COSMC play in O-glycan extension. Deleterious mutations in *COSMC* result in proteasomal degradation of the core 1 synthase and expression of Tn and STn truncated O-glycans. (*B*) Heat-map summary of hypermethylation of *COSMC* promoter in pancreatic tumor tissues from nine cases with, and nine cases without, expression of T-synthase/core 1 and truncated Tn, STn O-glycans [immunohistochemistry (IHC)], respectively. (*C, Upper*) Example of IHC expression of core 1 synthase and truncated O-glycans Tn, STn, and ST/T in hypermethylated *COSMC* promoter in a primary (upper row) and metastatic (lower row) pancreas tumor. (*Lower*) Examples of hypomethylated *COSMC* promoter in a primary (upper row) and metastatic (lower row) pancreas tumor. (*D*) Migratory (*Left*) and invasive (*Right*) properties of T3M4 wild-type, *COSMC* KO, and *COSMC* reexpression (CR) cells quantified following transwell migration ($n = 3$) and invasion through matrigel ($n = 3$). Significantly increased migration and invasion were observed in KO cells compared with wild-type and *COSMC* reexpresseion (CR) cells. (*E*) Significantly increased pancreatic tumor volume (mm^3) (*Left*) and tumor weight (*Right*) in KO cells ($n = 15$) compared with wild-type ($n = 10$) and *COSMC* reexpression (CR) ($n = 15$) cells with orthotopic T3M4 tumor cell implantation. (*F*) IHC demonstrating high expression of STn in T3M4 *COSMC* KO implanted mouse pancreas tumor tissues and reduced expression in implanted T3M4 wild-type and CR cells.

mechanisms, including altered expression of glycosyltransferases acting in the processing step (17), somatic mutations or hypermethylation of *COSMC* (13–15, 18), relocation of polypeptide GalNAc-transferases from Golgi to endoplasmic reticulum (ER) (19, 20), general reorganization of glycosyltransferase topology (19, 21), and fluctuations in cellular pH (22, 23). Although none of these possibilities are mutually exclusive and may in fact rule in different circumstances, the mechanism and the biological significance of the truncated O-glycophenotype have not been addressed widely in well-defined clinical and experimental systems.

Here, we first explored the genetic basis for expression of Tn and STn in pancreatic cancers by exome sequencing of over 200 genes involved in glycosylation and found essentially no evidence of somatic mutations in 46 cancers. We then determined that almost 40% of the cancers exhibited hypermethylation of the *COSMC* gene and that hypermethylation correlated with expression of truncated O-glycans as well as loss of C1GalT1 enzyme expression. This correlation suggested that inactivation of COSMC and core 1 O-glycan elongation is at least a prevailing mechanism in pancreatic cancer, and we therefore developed model systems with inactivation of COSMC to address the biological consequence. We used precise gene editing of a pancreatic cancer cell line (T3M4) to knockout *COSMC* to demonstrate that loss of COSMC induces enhanced growth and invasive properties in culture and as xenografts. We further developed an organotypic epidermis tissue model using the immortalized and nontumorigenic human keratinocyte (HaCaT) to produce an isogenic HaCaT cell model with and without COSMC, and demonstrate that loss of COSMC induces traditional oncogenic features, including hyperproliferation, loss of tissue architecture and disruption of basement membrane adhesion, and invasive growth. Finally, we performed a comprehensive polyomic approach, including O-glycoproteomics, transcriptomics, and quantitative phosphoproteomics studies, that provides support for a direct role of loss of COSMC in preventing cell–cell interactions and contact inhibition of cell growth.

Results

We have access to a large and unique cohort of patients with pancreatic cancer. To explore the genetic basis for the dramatically altered O-glycosylation pattern in human cancer, we performed exome-sequence analysis of 201 glycosylation genes (*SI Appendix*, Table S1) of 46 independent paired sets of normal tissue and pancreatic cancer. Pancreatic cancer is a cancer type known to abundantly express truncated Tn and STn O-glycans (24) (Fig. 1*A*). Surprisingly, we found only a few mutations in glycosylation genes and remarkably no mutations in the *COSMC* gene (*SI Appendix*, Fig. S1), previously proposed to harbor deleterious mutations in cancer (15). As a control, the expected frequency of somatic mutations was identified in K-ras (90%) (*SI Appendix*, Table S2) and p53 (50%) (*SI Appendix*, Fig. S1) in the cancer tissues (25). Given the high incidence of expression of truncated O-glycans in the evaluated pancreatic tumors and the fact that *COSMC* expression was reported to be epigenetically silenced in a human lymphoma cell line (26), we therefore investigated this possibility and found methylation of the promoter region of *COSMC* in 38% (13/34) of the pancreatic cancer tissue samples. Moreover, promoter methylation was shown to correlate with loss of C1GalT1 expression and presence of truncated O-glycans in these tissue samples (Fig. 1 *B* and *C*).

Truncated O-Glycans Promote Proliferation, Prevent Differentiation, and Induce Invasive Behavior. To explore potential biological roles of loss of elongated O-glycans, we first developed an isogenic cell model in the T3M4 pancreatic cancer line with and without elongated O-glycans using Zinc-finger nuclease (ZFN) disruption of *COSMC* (27). *COSMC* knockout cells expressing truncated O-glycans (*SI Appendix*, Fig. S2), exhibited enhanced invasive properties in culture (Fig. 1*D*) and enhanced growth and invasion as xenografts (Fig. 1 *E* and *F*). Effects were fully reversible upon reexpression of *COSMC* (Fig. 1 *D–F*). These results show that truncation of O-glycans exacerbates malignant and metastatic tumor behavior in the pancreatic cell line T3M4.

To explore biological effects at earlier stages of cancer progression, we developed an isogenic cell model in a spontaneously immortalized but nontumorigenic human epidermal keratinocyte cell line, HaCaT, which is a close approximate to normal

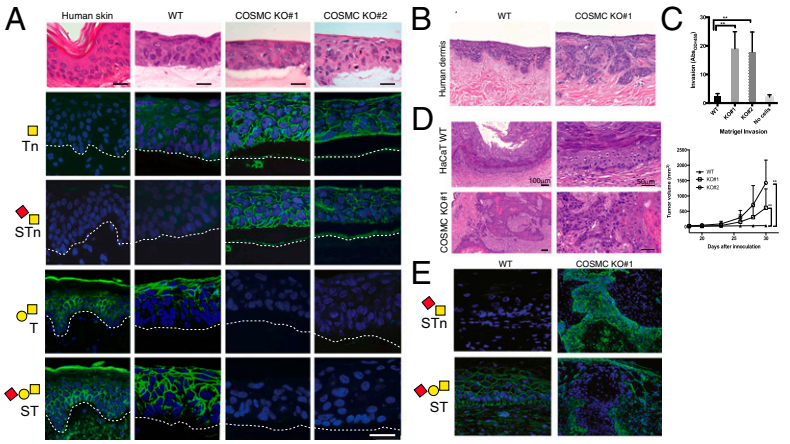

Fig. 2. Human immortalized keratinocyte HaCaT cells with *COSMC* KO develop a dysplasia-like phenotype when grown in 3D cultures. (*A*) H&E sections of HaCaT cells lacking elongated O-linked glycans (*COSMC* KO) grown in 3D cultures on collagen or human acellular human dermis develop a dysplasia-like phenotype, with poorly organized epithelium and impaired contact of basal cells to underlying collagen (*Lower Middle* and *Left*) (collagen gels; $n = 5$; see additional clones in *SI Appendix*, Fig. S3*C*) and invasion (human dermis) ($n = 2$). Normal human skin is stained as comparison. Corresponding micrographs are shown in the lower four rows stained with mAbs to defined carbohydrate structures [Tn, mAb 5F4; STn, mAb 3F1; T, mAb 3C9; ST, mAb 3C9 plus neuraminidase (Neu)]. Skin and wild-type HaCaT cells express the ST structure (NeuAcα2,3Galβ1,3GalNAc) whereas *COSMC* knockout cells simplify all O-glycosylation to GalNAc (Tn) and NeuAc-GalNAc (STn). Similar staining pattern was observed for KO#3, KO#4, and KO#5). (Scale bars: 50 μm.) (*B*) H&E sections of HaCaT cells lacking elongated O-linked glycans (*COSMC* KO) grown in 3D cultures on human acellular human dermis develop a dysplasia-like phenotype with invasion in underlying dermis. (*C*) Invasion was confirmed in matrigel invasion assay ($n = 3$, $^{**}P < 0.01$). (*D*) Inactivation of *COSMC* in HaCaT cells induces an invasive phenotype after s.c. inoculation in immune-deficient NOD.Cg-PrkdcscidB2mtm1Unc/J (NOD/SCID-B2m$^{-/-}$) mice and increased growth ($n = 6$). HaCaT KO cells proliferated diffusely in solid or trabecular patterns with stromal fibroblasts among the cancer cells (*Lower*) whereas HaCaT WT cells preserved their skin/keratinocyte cell nature with normal differentiation (*Upper*). (Scale bars: 50 μm and 100 μm, respectively.) A clear growth advantage was noted for *COSMC* KO cells compared with wild-type cells ($^{**}P < 0.01$). (*E*) HaCaT WT and KO xenografts stained with mAbs to defined carbohydrate structures [STn, mAb 3F1; ST, mAb 3C9 plus neuraminidase (Neu)].

keratinocytes with retained capacity to reconstitute a well-structured epidermis in vivo and ex vivo (28). HaCaT undergoes normal differentiation in organotypic cultures to form a stratified squamous epithelium and expresses O-glycans in a differentiation-dependent manner similar to human skin (Fig. 2*A*) (28). This ability provides a strong rationale for using the keratinocyte skin model to study the effect of the expression of cancer-associated glycans in complex cultures of normally differentiating epithelial cells. We first developed HaCaT cell lines with and without truncated O-glycans using ZFN disruption of *COSMC* (*SI Appendix*, Fig. S3 *A* and *B*). Tissue generated from wild-type HaCaT cells attached to and exhibited an appropriate epithelial–mesenchymal barrier (Fig. 2*A*). The organotypic skin cultures showed a histological differentiation pattern analogous to that of normal skin (Fig. 2*A*), except for the lack of a well-defined stratum corneum, as previously described (28, 29). In contrast, organotypic cultures built with HaCaT expressing truncated O-glycans (*COSMC* KO) revealed disrupted polarity and epithelial stratification, hyperchromatic nuclei, and variable cell sizes, features resembling those seen in dysplastic tissue (Fig. 2*A*). We also observed a loss of attachment between the epithelial and mesenchymal compartment when cells were grown on fibroblast containing collagen gels (Fig. 2*A* and *SI Appendix*, Fig. S3*C*). When cells were grown on human acellular extracellular matrix derived from human dermis, COSMC knockout cells invaded the dermal compartment whereas wild-type cells did not (Fig. 2*B*). The invasive properties of HaCaT cells with truncated O-glycans were confirmed by a matrigel invasion assay (Fig. 2*C*) and further compared in a murine xenograft model (Fig. 2*D*). When injected s.c., wild-type HaCaT cells formed skin-like tissue with normal basal cells respecting the dermal–epithelial border and terminal differentiation with keratinization (Fig. 2 *D* and *E*). In contrast, the isogenic *COSMC* mutant HaCaT cells expressing truncated glycans demonstrated accelerated growth (Fig. 2 *D* and *E*), with disorganized tissue borders and invasion of surrounding muscles and vessels (Fig. 2*D*). These results demonstrate that truncation of O-glycans directly induces classical oncogenic features.

Additional evidence of oncogenically transformed properties was provided by the results of comparative whole-genome transcriptomic analyses of the isogenic HaCaT cell lines (*SI Appendix*, Table S3), which revealed increased expression of gene clusters linked to proliferation when elongated O-linked glycans were eliminated (Fig. 3*A* and *SI Appendix*, Table S3). Concomitantly, there was increased proliferation of *COSMC* mutant clones under conventional cell-culture conditions (Fig. 3*C*, $P < 0.05$) and staining of the organotypic cultures with a marker for proliferation, Ki-67 (Fig. 3*D*). The proliferative cells were localized throughout the organotypic epithelium for *COSMC* mutant cells whereas wild-type cells displayed Ki-67 only in basal cells (Fig. 3*D*), similar to that seen in normal skin. Gene-expression profiles demonstrated down-regulation of genes involved in terminal epithelial differentiation in *COSMC* mutant cells (*SI Appendix*, Table S3 and Fig. 3*B*). This effect on terminal differentiation was verified in organotypic cultures by immunodetection of terminal differentiation markers, keratin-10, and involucrin (Fig. 3 *E* and *F*). Additional evidence for lack of differentiation of HaCaT cells with truncated O-glycans included the observed down-regulated expression of Notch, p53, IRF6, and Foxo3 with simultaneous up-regulation of the expression of Δ*N*p63 and IKBKG, an expression pattern that has previously been associated with stem cell-like properties (Fig. 3*G* and *SI Appendix*, Table S3) (30). Concordantly, global RNA sequencing of the isogenic pancreatic cell lines T3M4 (*SI Appendix*, Fig. S4 and Table S4) revealed that expression of genes associated with differentiation, cell death, and apoptosis was down-regulated; and genes associated with cellular movement and cell proliferation were up-regulated in T3M4 *COSMC* knockout cells (*SI Appendix*, Fig. S5 and Table S5).

Identification of Specific O-Glycosylation Sites by Global Glycoproteomics. To identify proteins involved in the induction of oncogenic features by truncation of the O-linked glycans, we performed an extended search for O-glycosylated proteins and the individual O-glycosylation sites in HaCaT *COSMC* cells and their secretions (Fig. 4*A*). We recently developed a method using lectin affinity chromatography enrichment, followed by identification of GalNAc O-glycopeptides by nLC-MS/MS, with electron transfer dissociation (ETD) used to specify sites of O-glycosylation (Fig. 4*A*) (27, 31). Here, we performed an expanded in-depth analysis of the O-glycoproteome of HaCaT cells (Fig. 4*A* and *SI Appendix*, Table S6) to further elucidate the molecular processes that cause the observed oncogenic transformation. The analysis resulted in identification of 446 O-glycoproteins and 1,471 O-glycosites, of which only 369 were previously annotated (*SI Appendix*, Table S6). Almost 50% of the identified glycoproteins showed only a single glycosite common to both HaCaT and T3M4 cells (*SI Appendix*, Table S6) [due to a regrettable error the pancreatic cell line denoted Capan-1 in our previous studies (27, 32) has been shown to be T3M4] and included representations of glycosylation

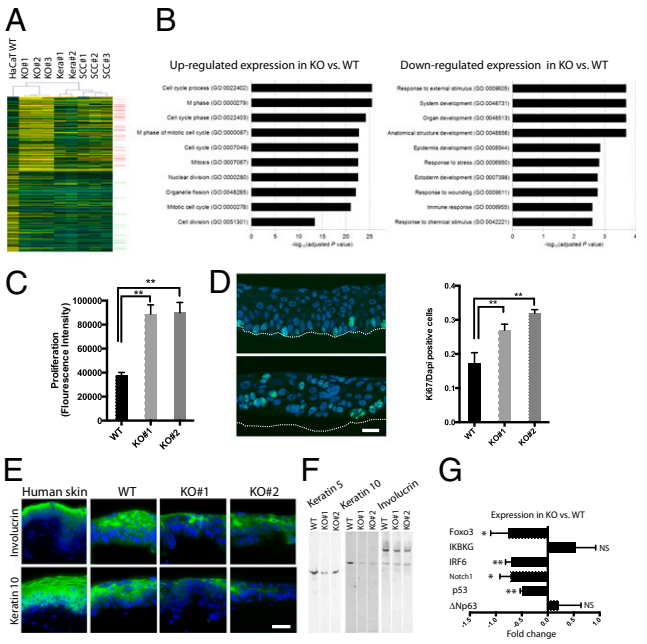

Fig. 3. (*A*) RNA expression profiles compared between HaCaT WT and *COSMC* KO cells compared with expression profiles in human keratinocytes (Kera) and squamous skin carcinoma cells (SCC1 to -3) (for a complete list, see *SI Appendix*, Table S3). Genes involved in mitosis (GO:0007067) are indicated by red lines, and genes involved in epidermal development (GO:0008544) are indicated by green lines. (*B*) Up-regulated and down-regulated gene classes in *COSMC* knockout cells vs. wild-type HaCaT cells grown under conventional conditions. Epithelial cells lacking elongated O-linked glycans down-regulate genes involved in keratinocyte development and up-regulate genes involved in proliferation. (*C*) Proliferation assay showing 2.5-fold increased proliferation of *COSMC* KO#1 and KO#2 compared with HaCaT WT ($n = 5$). (*D*) IHC of organotypic skin equivalent cultures with the Ki-67 proliferation marker demonstrate enhanced proliferation and altered topology of the proliferation layer. Ki-67–positive fraction of DAPI-positive cells in *COSMC* KO shown at the *Right* ($n = 3$). (Scale bar: 30 μm.) (*E*) IHC demonstrates down-regulation of keratin 10 and dispersion of involucrin. (Scale bar: 50 μm.) (*F*) SDS/PAGE Western blotting of keratin 10 and unchanged keratin 5 expression ($n = 3$). (*G*) Expression profiles showed down-regulation of Notch, p53, IRF, and Foxo-3 with simultaneous up-regulation of IKBKG: an expression pattern associated with lack of differentiation and stem cell-like properties (error bars show 1× SD of replicates; $*P < 0.05$, $**P < 0.01$; NS, nonsignificant).

involved in adhesion (Fig. 4*B*), including CD44, integrins, desmogleins, and other cell-surface adhesion molecules known to play roles in cancer (33).

Quantitative Phosphoproteomics Identifies Adhesive Functions and Downstream Signaling Pathways Affected by Truncation of O-Glycans. To examine the main signaling pathways affected by truncation of O-glycans, we next investigated the steady-state phosphorylation status of the HaCaT cells by global quantitative phosphoproteomics using stable isotope labeling by amino acids in cell culture (SILAC) (34–36) (Fig. 4*C*). Two biological replicates of HaCaT cells reproducibly identified 8,013 unique phosphorylated sites that were assigned to phosphopeptide sequences with high confidence (class I) (*SI Appendix*, Fig. S5 and Table S7) on 2,272 different proteins. The distribution of Tyr(P), Thr(P), and Ser(P) was 0.3%, 8.7%, and 91.0%, respectively (*SI Appendix*, Fig. S5), which is comparable with previous observations (34). We identified 294 up-regulated phosphorylated and 397 down-regulated sites (more than twofold) common for two independent HaCaT *COSMC* knockouts (*SI Appendix*, Table S8). Our analysis revealed altered regulation of proteins involved in cellular adhesion and RAS signaling, including up-regulation of PAKs, PKC-α, PKC-β, DMPK, and CLK3 in HaCaT cells with truncated O-glycans (Fig. 4 *D* and *E* and *SI Appendix*, Fig. S6 and Table S8), and down-regulation of CK2A and CLK1 (*SI Appendix*, Fig. S6). Interestingly, we found changes in phosphorylation of a large proportion of proteins with a pattern linked to loss of cellular adhesion, such as ZO-1 involved in tight junctions, integrin β4 involved in hemidesmosome formation, the hyaluronan receptor CD44, desmogleins, desmocollins, and desmoplakins, as well as downstream protein networks involved in desmosome formation (Fig. 4 *C* and *D*, Table 1, and *SI Appendix*, Table S8). We did not perform a global phosphoproteomic screen of T3M4 cells. Instead, a focused analysis of phosphoprotein expression using the Kinetworks KPSS-1.3 Screen (*SI Appendix*, Table S9) demonstrated commonalities in adhesive functions and downstream activation of signaling pathways (PKCalpha, PKCbeta, integrin signaling) with selective up-regulation of nine phosphoproteins [PKBα (S473 and T308), GSK3β (S9 and Y216), S6Kb1, GSK3α (S21), PKCα/β2, and PKCα] (*SI Appendix*, Fig. S8).

Cancer-Associated Truncation of O-Glycans Impairs Cell–Cell Adhesion. The overrepresentation of O-glycoproteins and differentially phosphorylated proteins involved in cell adhesion (Table 1) suggests that truncation of O-glycans affects cell–cell adhesion. We therefore investigated the adhesive functions of HaCaT cells with truncated O-glycans, which were found to migrate individually into wounded areas, in contrast to the collective migration of their wild-type counterpart (Fig. 5*A*). Ultrastructural characterization confirmed the loss of structural integrity of the intercellular adhesive systems in organotypic keratinocyte cultures, with loosely packed *COSMC* KO mutant cells (Fig. 5*B*). Only minor morphological differences of the desmosomes were noted whereas there was increased intercellular space (asterisk in Fig. 5*B*), and diminished numbers of tight junctions (arrowhead in Fig. 5*B*) in organotypic cultures with HaCaT cells with truncated O-glycans. Moreover, HaCaT cells with truncated O-glycans readily dissociated during cell-dissociation assays (Fig. 5*C*), indicative of compromised intercellular adhesion. This compromised intercellular adhesion was confirmed by increased keratin retraction in *COSMC* KO cells grown either as monolayers or in organotypic cultures both on collagen and acellular dermis (Fig. 5 *D* and *E*) and suggests defects in desmoglein functions (37). Consistent with the influence of elongated O-glycans on cell–cell adhesion, we found that HaCaT cells with truncated O-glycans displayed compromised contact-mediated growth arrest (Fig. 5*E*). It has been shown that desmogleins are involved in the regulation of p38 MAPK activity, which controls keratin filament dynamics (37). Loss of desmoglein transinteraction triggers p38 MAPK activation and releases the anchoring of the keratin filaments (37). Interestingly, we found increased phosphorylation of p38 MAPK (MAPK14) (*SI Appendix*, Tables S7 and S8 and Fig. 5*F*) in *COSMC* KO compared with WT cells. We therefore hypothesized that the loss of elongated O-glycans affected the intercellular adhesion system of keratinocytes through p38. In accordance with this interpretation, treatment with the p38 inhibitor SB203580 prevented the observed loss of cell adhesion in *COSMC* KO cells and wild-type HaCaT cells treated with the p38 inducer anisomycin evaluated by a dispase-based dissociation assay (Fig. 5 *G* and *H*). The compromised adhesive system was suggested by the loss of tight junction protein 1 (ZO-1) (*SI Appendix*, Fig. S7*B*) and in cells with truncated O-glycans (*SI Appendix*, Fig. S7*A*) corresponding to the observed decrease in phosphorylation of zonula occludens protein, ZO-1 (Table 1 and *SI Appendix*, Tables S7 and S8).

Discussion

The aberrant expression of truncated O-glycans is a hallmark of epithelial cancers (3, 5–7, 38), and a number of mechanisms

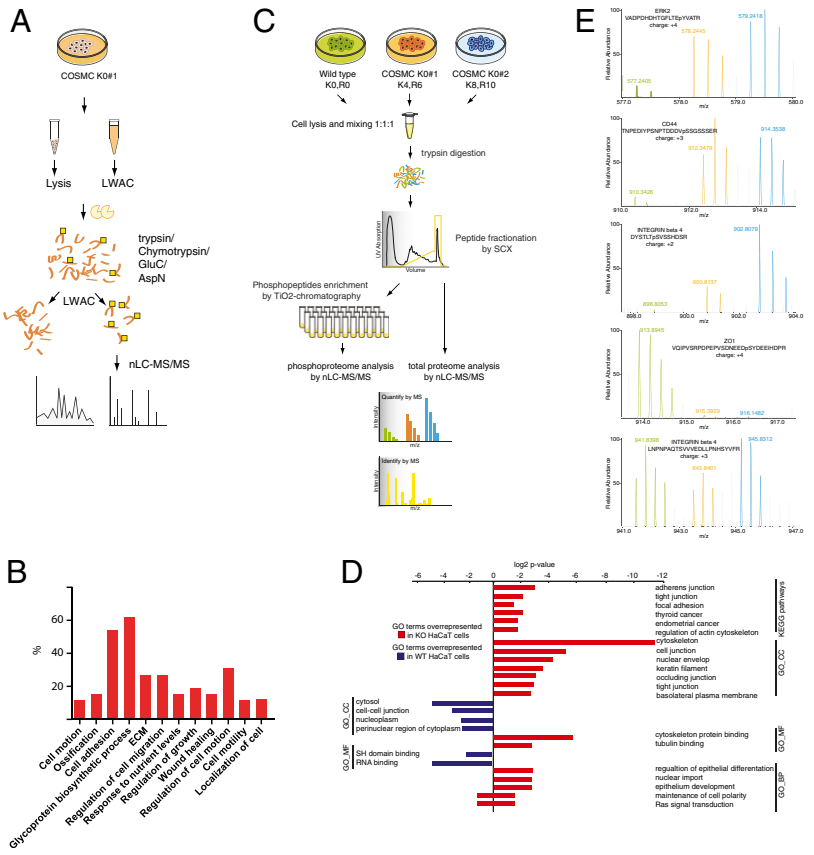

Fig. 4. O-proteomics and quantitative phosphoproteomics of *COSMC* knockout cells. (*A*) The O-GalNAc proteomics strategy. GalNAc-glycopeptides are isolated on lectin weak-affinity chromatography (LWAC) and separated by IEF before nanoflow liquid chromatography tandem mass spectrometry (nLC-MS/MS) analysis. We identified 446 O-glycoproteins and 1,471 O-glycosites, of which only 369 were previously annotated in UniProt and O-GLYCBASE. (*B*) Global gene ontology (GO) analysis identified cellular components that carry O-linked GalNAc, including cell-adhesion proteins. Comparison was made with the total human proteome and expressed as a percentage. (*C*) Quantitative phosphoproteomics of *COSMC* KO cells versus WT. Experimental design of MS-based quantitative phosphoproteomics analysis by SILAC. Three populations of cells were labeled with normal and stable isotope-substituted arginine and lysine, creating proteins and peptides distinguishable by mass. (*D*) Global gene ontology (GO) analysis of the regulated set of phosphoproteins identified adhesive proteins, RAS signaling, epithelial development, and differentiation as enriched terms. Red bars represent GO terms overrepresented in WT HaCaT cells whereas blue bars represent GO terms overrepresented in KO HaCaT cells. log2 transformation of *P* value is indicated. (*E*) Illustrative examples of high-resolution MS spectrum are shown: Erk2, CD44, integrin-β4 with an increase, and ZO-1 with a decrease in phosphorylation at selective sites in mutant compared with wild-type cells. For integrin-β4, we also show an unmodified peptide with no regulation between the three conditions.

leading to the expression of truncated glycans have been put forward (13–15, 17–23). Disruptive mutations, as well as hypermethylation of the chaperone COSMC required for O-glycan elongation, have been proposed as mechanisms (13–15, 18), and here we could confirm in a large clinical study of pancreatic cancers that hypermethylation and not somatic mutations in COSMC is indeed a major cause for expression of the truncated Tn and STn O-glycans. Other mechanisms, including altered expression of enzymes involved in elongation and sialylation and relocation of the enzymes initiating O-glycosylation (GalNAc-Ts) from Golgi to ER, may also play roles (20), and it has previously been reported that forced expression of GalNAc-Ts in ER influences invasive and metastatic growth of tumor cells (19). However, the key question—whether the characteristic expression of Tn and STn truncated O-glycans in cancer intrinsically has biological roles for the malignant process—has remained unanswered.

Given the prevalence of COSMC hypermethylation found in pancreatic cancer, we therefore wanted to develop cell systems that unequivocally could address the functional role of loss of COSMC in cancer. Although tumors generally express Tn and STn O-glycans (1–7), most established cancer cell lines generally do not express substantial amounts of these antigens unless the cell lines have *COSMC* mutations (32). We first used ZFN gene editing to develop an isogenic pancreatic cancer cell line model, with and without homogenous expression of truncated O-glycans, and demonstrated that the COSMC mutant exhibited increase proliferative and invasive properties. We next took the isogenic cell system into an organotypic model using a well-differentiated immortalized but nontumorigenic human keratinocyte HaCaT isogenic cell line to address the biological roles of truncated O-glycans in the development of human cancer. Using this organotypic model, we demonstrated that loss of COSMC affects epithelial tissue integrity and homeostasis. Moreover, although HaCaT normally is nontumorigenic in nude mice without, e.g., transfection with the HRAS oncogene (39, 40), we found that HaCaT with deficiency in COSMC was highly tumorigenic. Thus, we believe that the results, for the first time to our knowledge, demonstrate in well-defined cell systems that expression of truncated glycans plays a direct role in induction of oncogenic features of cell growth and invasion, including disruption of contact between the epithelium and the dermal compartment and loss of cell–cell adhesion.

HaCaT cells constitute an immortalized cell line, most likely due to point mutations in p53, that has become a frequently used model system to study keratinocyte biology and transformation (41). Importantly, HaCaT cells retain a stable chromosome content and remain nontumorigenic throughout 320 passages (29), and, when grown in organotypic cultures, HaCaT cells form differentiated skin, express terminal differentiation markers, and exhibit normal substratum adhesion and cell spreading required for proliferation and prevention of apoptosis (28, 42, 43). Tumorigenic conversion of the HaCaT cells has been observed after transfection with vH-ras oncogene (39), increased activation of tyrosine kinase receptor PDGF (44–48), and loss of adhesion (49, 50). These phenotypic characteristics are the same that we observe when truncating the O-linked glycans by *COSMC* knockout. Wild-type HaCaT cells are very similar to primary human keratinocytes, as demonstrated by their similar RNA expression profiles (Fig. 3*A*). In contrast, HaCaT cells with deficiency in COSMC had increased expression of genes related to cellular movement and proliferation whereas genes linked to differentiation and apoptosis were down-regulated (Fig. 3*A*). These changes are similar to expression profiles observed in squamous cell carcinoma cells, further supporting the oncogenic phenotype induced by *COSMC* knockout.

How does loss of COSMC exert such profound biological effects on cell behavior? COSMC serves as a private chaperone of C1GalT1, and elimination of the gene function will only result

Table 1. Differential phosphorylation of adhesion proteins in COSMC KO HaCaT cells compared with WT

Protein name	Gene name	AA position	Ratio cl1/WT*	Ratio cl2/WT*
ECM and intercellular adhesion				
CD44 antigen	CD44	S697	**2.61**	**2.63**
Desmosome proteins				
Desmocollin-2	DSC2	S803	**1.71**	**1.57**
Desmocollin-2	DSC2	T800	**1.71**	**1.57**
Desmoglein-4	DSG4	T781	**2.44**	**1.51**
Desmoplakin	DSP	S32	**1.79**	**2.04**
Desmoplakin	DSP	S176	**1.54**	**1.59**
Desmoplakin	DSP	Y28	**1.49**	**1.22**
Adherens junction proteins				
Catenin alpha-1	CTNNA1	T654	**1.97**	**1.81**
Catenin alpha-2	CTNNA2	S651	**2.01**	**1.8**
Catenin alpha-2	CTNNA2	T653	**1.84**	**1.64**
Catenin beta-1	CTNNB1	S552	**2.48**	**2.01**
Focal adhesion proteins				
Integrin beta-4	ITGB4	S1501	**3.42**	**8.98**
Integrin beta-4	ITGB4	S1486	**3.27**	**12.35**
Integrin beta-4	ITGB4	S1483	**3.22**	**11.5**
Integrin beta-4	ITGB4	T1512	**3.15**	**13.1**
Integrin beta-4	ITGB4	T1487	**2.86**	**9.01**
Integrin beta-4	ITGB4	S1515	**2.58**	**6.32**
Integrin beta-4	ITGB4	S1494	**2.43**	**5.12**
Integrin beta-4	ITGB4	S1498	**1.73**	**5.95**
Integrin beta-4	ITGB4	S1518	**1.72**	**4.55**
Integrin beta-4	ITGB4	S1454	**1.44**	**3.34**
Integrin beta-4	ITGB4	S1457	**1.32**	**3.36**
Integrin beta-4	ITGB4	S1521	**1.31**	**4.08**
Tight junction proteins				
Tight junction protein ZO-1	TJP1	S135	*0.41*	*0.39*
Tight junction protein ZO-2	TJP2	S1009	*0.5*	*0.39*
Tight junction protein ZO-2	TJP2	T476	*0.7*	*0.51*
Tight junction protein ZO-2	TJP2	S463	*0.78*	*0.59*
Tight junction protein ZO-2	TJP2	S446	*0.81*	*0.53*

*Up-regulated phosphorylation sites are marked in bold, and down-regulated phosphorylation sites are marked in italics.

in global loss of biosynthesis of core 1 O-glycan structures on all O-glycoproteins, whereas glycosylation of all other glycoproteins is expected to be unaltered (14). This loss of core 1 O-glycan structures was confirmed in both HaCaT and T3M4 cells, in which elimination of COMSC resulted in expression of STn and Tn structures. The predominant expression of the cancer-associated structures Tn and STn strongly suggests that these structures drive the observed cancer phenotype. However, we cannot completely exclude that the observed phenotype in *COSMC* KO cells is due to other effects of COSMC, besides acting as a private chaperone for the core 1 synthase. It should be emphasized, however, that our results show and confirm previous findings that it is *COSMC* that is dysregulated in cancer and not the C1GALT1 gene. The presented strategy will now allow us to dissect the function of COSMC and the individual glycan structures using targeted elimination of the glycosyltransferases responsible for each step in the elongation process. This approach will generate cells selectively presenting Tn, STn, and T structures and allow the comparison of phenotypes with COSMC knockout cells. Furthermore, introduction of the core 3 synthase will allow us to examine whether the cancer phenotype is due to loss of core 1 structures or the de novo presentation of Tn and STn structures. We hope that such future studies will help to establish the function of each individual glycan structure in development of the cancer phenotype using our organotypic skin model.

Because loss of COSMC produces global affects on O-glycosylation of proteins, it is not straightforward to decipher the specific molecular mechanisms and individual O-glycoproteins underlying the observed oncogenic features induced: more than 80% of the human proteome that enters and passes through the secretory apparatus is predicted to be O-glycosylated (32). However, the isogenic cell model systems developed here now enable us to begin to address biological pathways affected by the single loss of the *COSMC* gene on a global Ome-wide level. We first characterized the O-glycoproteome of HaCaT and T3M4 cells (Fig. 3 and *SI Appendix*, Table S4) and demonstrated that many proteins playing central roles in cell–cell adhesion, differentiation, and normal development of human tissue are indeed O-glycosylated. Many newly discovered O-glycoproteins were common to both HaCaT and T3M4 cells, and common O-glycoproteins included CD44, integrins, desmogleins, and other cell-surface adhesion molecules known to play roles in cancer (33). We and others have demonstrated that site-specific O-glycosylation of proteins can have profound effects on protein functions, including affecting proprotein processing, modulation of ligand-binding properties of receptors, and regulation of ectodomain shedding and cell signaling (51–55). Moreover, a recent study demonstrated that site-specific O-glycosylation in the stem region of the gCSF receptor regulated homodimerization and signaling of this receptor and that a common somatic mutation in a single O-glycosite was a cancer driver in a large percentage of patients with chronic neutrophilic leukemia (56).

We next examined the effects of truncated O-glycans on cell signaling in general using a global comparative quantitative phosphoproteomic analysis of the isogenic HaCaT cell model (34–36). The analysis demonstrated changes in regulation of proteins involved in cellular adhesion and RAS signaling. We found changes in phosphorylation of a large proportion of proteins in HaCaT cells whose functions are linked to loss of cellular adhesion, including decreases in phosphorylation of zonula occludens protein, ZO-1, and increased phosphorylation of integrinß4, desmogleins, desmocollins, and other proteins involved in intercellular adhesion (Table 1). Consistent with the importance of O-linked glycans in intercellular adhesion in general and desmoglein function in particular, we found that loss of elongated O-glycans increased phosphorylation of p38 MAPK and released the anchoring of the keratin filaments. This loss of adhesion was reverted by treatment with a p38 inhibitor, showing that the intercellular adhesion system of keratinocytes through p38 MAPK represent one key event affected by loss of *COSMC* function (see model in *SI Appendix*, Fig. S6*D*). Desmoglein-3 is known to regulate cell–cell adhesion through p38 MAPK activation (37), and the finding of a specific O-glycan on desmoglein-3 may furthermore suggest that truncation of O-glycans affects desmoglein-3 function directly.

In addition, we found hyperphosphorylation of CD44 in HaCaT knockout cells. Hyperphosphorylation of CD44 is linked to growth-permissive functions through the tumor suppressor NF2/Merlin by activation of the RAS-ERK pathway (33). Consistent with an activation of the ERK pathway, we also found increased activation of the ERK1/2 pathway (*SI Appendix*, Fig. S7*B*) in *COMSC* knockout HaCaT cells. The activation of ERK could, however, also be a secondary effect to the loss of adhesion (57) or a direct effect of truncated O-glycans on the receptor molecules themselves, which could be mediated by several mechanisms. The possibilities include coregulatory roles of glycans on regulated ectodomain shedding (53), as well as an influence on receptor homodimerization (56).

To our knowledge, our study presents the first Ome-wide view of loss of COSMC and truncation of O-glycosylation in well-defined cell systems. Consistently, we demonstrate that truncation of O-glycans influences several important pathways in tissue homeostasis and oncogenesis, including adhesive and signaling

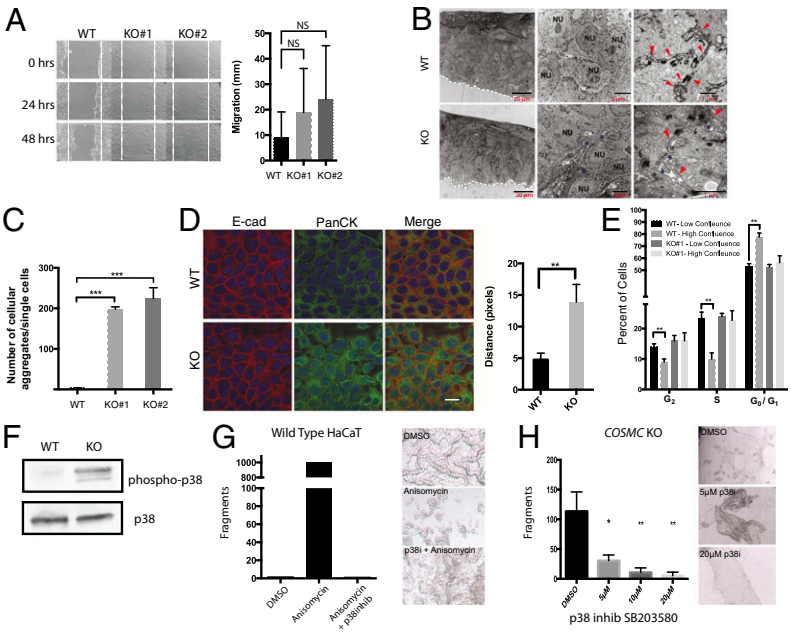

Fig. 5. Truncation of O-linked glycans down-regulates intercellular adhesion. (*A*) *COSMC* KO cells migrated as noncoherent single cells compared with wild-type HaCaT cells in contact-inhibited monolayer cultures after scratch wound ($n = 3$). (*B*) Transmission electron microscopy micrographs of HaCaT wild-type and COSMC KO organotypic cultures. Overview of all cell layers is shown *Left*. Increased magnification with illustration of 5–8 cells is shown *Center*. (Right) Increased magnification of cell–cell interface. Increased intercellular space is noted between COSMC mutant cells (asterisks) whereas tight interaction is seen between wild-type cells (marked with arrowheads) (CM, cell membrane; NU, nucleus). (*C*) Cell-dissociation studies confirmed lack of cell–cell adhesion in *COSMC* KO HaCaT cells. Epithelial sheets of HaCaT WT cells resisted mechanical stress whereas *COSMC* KO HaCaT cells did not ($n = 3$) (***$P < 0.001$). (*D*) Keratin retraction (green) indicative of loss of desmoglein function in *COSMC* KO HaCaT cells. E-cadherin staining (red), which was only mildly affected, served to delineate cell membranes ($n = 2$). Keratin retraction was quantified by measuring the distance between the mass of the keratin bundles in areas of similar cell density as described in ref. 37 (**$P < 0.01$). (Scale bar: 20 μm.) (*E*) Number of WT and *COSMC* KO cells in the cell-cycle phases ($G_{1/0}$, G_2, and S phase), when grown under low and high confluence. No change was observed in the number of *COSMC* KO cells in $G_{1/0}$, G_2, and S phase under high vs. low confluence, suggesting compromised contact inhibition ($n = 3$) (**$P < 0.01$). (*F*) p38 MAPK activation was observed in COSMC KO cells compared with wild-type cells. (*G*) Loss of cell adhesion in wild-type HaCaT cells treated with anisomycin (80 μg/mL) was prevented by SB203580 as detected by dispase-based dissociation assays ($n = 3$) ($P < 0.001$; anisomycin plus p38 inhibitor vs. anisomycin). (*H*) Loss of cell adhesion in COSMC KO was prevented by SB203580 as detected by dispase-based dissociation assays ($n = 3$) (*$P < 0.05$; **$P < 0.01$; DMSO vs. p38 inhibitor).

molecules, which suggests that cancer cells truncate their O-glycans to affect multiple systems simultaneously to promote tumor formation. However, this also makes it less likely to identify a single pathway that is affected by truncation of O-glycans. Further dissection of the interplay between the O-glycosylation and the observed oncogenic features will require deciphering specific effects of O-glycans on specific O-glycoproteins. The organotypic model presented here now enables future studies of site-specific glycosylation by use of precise genome-editing techniques to probe the role of individual glycosyltransferases for the observed invasive cancer phenotype. In addition, this tissue model will be a powerful tool to discover general biological functions of glycosylation in epithelial homeostasis, epithelial differentiation, and cancer development. Finally, the truncation of O-glycans has implications for the formation of tumor-specific glycopeptidic neoepitopes consisting of a monosaccharide and a specific wild-type protein sequence (9). Such neoepitopes represent potential targets for monoclonal antibody therapy (10, 58), and our findings provide support for immunotherapeutic strategies targeting aberrant O-glycoproteins.

In conclusion, we present evidence that the characteristic truncation of O-glycans found in pancreatic and most epithelial cancers is not due to somatic mutations, but is at least partly caused by epigenetic silencing of the *COSMC* chaperone gene by promoter hypermethylation. We demonstrate that loss of COSMC intrinsically induces an oncogenic phenotype characterized by increased proliferation, compromised adhesion, and invasiveness (28, 41). Our study demonstrates the importance of COSMC and glycosylation as a key regulator of the malignant phenotype and suggests that overexpression of truncated O-glycans is an early and sustained event during cancer development that provides a permissive environment for malignant evolution during the progression to metastasis.

Methods

Human Rapid Autopsy Samples and DNA Isolation. Human pancreatic tumor, metastases, and uninvolved normal tissues were acquired with consent and Institutional Review Board approval from de-identified pancreatic cancer patients through the Rapid Autopsy program at the University of Nebraska Medical Center (UNMC). Genomic DNA was isolated from the tumor ($n = 46$) and uninvolved normal ($n = 46$) tissues of pancreatic adenocarcinoma patients using Maxwell 16 tissue DNA isolation kits (Promega Corporation). The isolated DNA was used for next-generation exome sequencing, ICE COLD PCR, and combined bisulfite restriction analysis.

Library Construction and Sequencing for Exome Capture. Sequencing exome capture was performed using a NimbleGen exome capture protocol (NimbleGen SeqCap EZ Library, www.nimblegen.com/products/seqcap/ez/index.html). In brief, qualified genomic DNA samples were randomly fragmented by the Covaris AFA process (http://covarisinc.com/), adapters ligated to both ends, amplified by ligation-mediated PCR (LM-PCR), purified, and hybridized to the NimbleGen1.68M target region array for enrichment. Both non-captured and captured LM-PCR products were subjected to quantitative PCR to estimate the magnitude of enrichment. Captured libraries were loaded onto the Illumina HiSeq2000 platform. High-throughput sequencing was independently performed on each captured library to ensure that each sample met the 100× coverage. Raw image files were processed by Illumina base-calling software version 1.7 with default parameters, and the sequences of each individual were generated as 90-bp paired-end reads.

Data Filtration and Alignment. The raw HiSeq2000 sequencing reads were initially filtered to exclude contaminating reads representing sequencing primers or low-quality reads. Read pairs were retained only if both reads from one pair matched the following criteria: (*i*) no occurrence of sequencing contaminating primers; (*ii*) the proportion of bases with quality ≥ 5 was no less than 50%; and (*iii*) the proportion of unidentified bases (N base) was less than 10%. Afterward, high-quality sequencing reads were aligned to the human genome hg19/GRCh37 using BWA 0.5.9-r16 (Burrows-Wheeler Aligner) with the following parameters: bwa aln -o 1 –e 50 –m 100000 –t 4 –i 15 –q 10 -l, generating the initial BAM files, followed by additional realignment to the BAM files to get the most reliable alignment results using the Genome Analysis Toolkit (GATK) (59).

Identification of Somatic Nucleotide Variations. VarScan (60) v2.2.5 was used to detect potential somatic nucleotide variations (SNVs) with the command: –min-coverage 10–min-coverage-normal 10–min-coverage-tumor 10–min-var-freq 0.1–min-freq-for-hom 0.75–somatic-p-value 0.05. SNVs were scored under the following criteria: (*i*) coverage should be ≥10 in normal and ≥10 in tumor; (*ii*) the variant frequency should be <2% in normal and ≥10% in tumor; and (*iii*) *P* value to call a somatic site was <0.05.

Identification of Small Insertions/Deletions. Somatic insertions/deletions (InDels) were identified by realignment of the BWA-aligned reads followed by GATK (59, 61) analysis using default "SomaticInDelDetector" command parameters enabling identification of somatic InDels by comparing tumor tissue with matched normal tissue. Somatic InDels were retained if they fitted the conditions: (*i*) reads depth (DP) >5 in both tumor and normal samples; (*ii*) average mismatch rate <0.5 in both normal and mutant alleles; (*iii*) average mapping quality >20 in both normal alleles and mutant alleles in tumor; and (*iv*) median InDel offsets from reads terminal >5 bp.

Analysis of DNA Methylation by Combined Bisulfite Restriction Analysis. *COSMC* genomic DNA sequences have CpG islands (CpG% = 22.7%, GC% = 66.9%%, observed CpG/Expected CpG = 1.01, length = 493) both upstream and downstream of transcription start site (TSS). Combined bisulfite restriction analysis was performed as described previously (62, 63). In brief, Genomic DNA was isolated from the tumor specimens as mentioned in *Human Rapid Autopsy Samples and DNA Isolation*. The isolated genomic DNA was treated with sodium bisulfite using the Epitect Bisulfite Kit (Qiagen). PCR primers were designed using MethPrimer, and CpG island-specific primers were used to amplify the bisulfite converted genomic DNA digested with Taq1 and Tail restriction enzymes. The following methylation-specific primers were used to amplify downstream and upstream of transcription start sites (TSSs): F5′-TGTAGTTAGAATAGTTTGGTTAGGA-3′, R5′-CCCTCTAAAAAACCAAAAAAAC-3′ (downstream of the TSS); and F5′-GGGGTATATTAGAGAAATTATTAAG-3′, R5′-AATTCAAAAACTTACTATAAACCTA-3′ (upstream of the TSS). A fully methylated genomic DNA sample was used as a control (New England Biolabs). PCR products were digested using the restriction enzymes TaqI or Tail (New England Biolabs and Fermentas, respectively). The digested products were loaded onto an 8% PAGE gel, separated by electrophoresis, and visualized with SYBR Green Gold (Life Technologies).

ZFN Transfection and Clone Selection. Transfection with ZFN constructs and subsequent cloning/selection were performed as described previously (27). Human keratinocyte cell line HaCaT cells (28) were transfected with mRNA (Sigma-Aldrich) or 5 μg of endotoxin-free plasmid DNA using nucleofection and the Amaxa Nucleofector (Lonza). *COSMC* knockout cells were selected by reactivity with mAbs to Tn and loss of reactivity with mAb to the C1GalT1 enzyme following single-cell cloning. Cells were transferred to diagnostic imaging printed slides (Clearcell; Histolab), fixed with acetone, incubated with mAbs overnight, and FITC-conjugated rabbit antibody to mouse IgG (Dako, Denmark) for 45 min, and mounted with ProLong Gold antifade reagent with DAPI (Invitrogen). Fluorescence microscopy was performed using a Zeiss Axioskop 2 plus with an AxioCam MR3. Bit depth and pixel dimensions were 36 bit and 1,388 × 1,040 pixels, respectively. Clones were confirmed to have *COSMC* mutations using PCR and sequencing using primers 5′-AGGGAGGGATGATTTGGAAG-3′ and 5′-TTGTCAGAACCATTTGGAGGT-3′. *COSMC* reexpression in T3M4 cells was performed with full-length *COSMC*. cDNA was amplified from Capan-2 cells, using the following primer sets: forward 5′-CGTGAGAGGAAACCCGTG-3′ and reverse 5′-TGTGTGGTTATACCAGTGCC-3′. The amplified *COSMC* cDNA was sequence-verified and cloned into the pLVX-Puro lentiviral vector expression system (Clontech) as per the manufacturer's instructions. *COSMC* and vector control lentiviral particles were produced in HT293A packaging cells and then transduced into T3M4 *COSMC* KO cells, followed by selection and maintenance in puromycin (3 μg/mL; Invivogen).

Reverse-Transcriptase PCR and PCR analysis. Total RNA isolation and cDNA conversion were performed using previously described methods (64). *COSMC*, *C1GalT-1*, and *GAPDH* mRNAs were amplified with specific primers and quantified as described previously (64).

RNA Expression Profiles of Normal and *COSMC* Knockout HaCaT Cells. RNA expression profiles of normal and *COSMC* knockout HaCaT cells were performed using Human Gene 1.1 ST arrays (Affymetrix). Data were RMA-normalized, and differentially expressed genes were identified using Rank Products implemented in MultiExperiment Viewer (65). The expression profiles of the differentially expressed genes were compared with expression profiles in normal keratinocytes (GEO accession numbers GSM852784 and GSM852785) and in squamous skin carcinoma cells (GEO accession numbers GSM852778, GSM852780, and GSM852782). GEO datasets and HaCaT datasets were normalized using cyclic loess implemented in the Limma package for R (www.R-project.org) and visualized in MultiExperiment Viewer. Gene set enrichment analysis of differentially expressed genes in *COSMC* knockout HaCaT cells was performed using WebGestalt.

RNA Sequencing, Network Analysis, and Quantitative Real-time PCR. Total RNA was isolated with TRI reagent (Molecular Research Center) from T3M4 wild-type and KO cells as per the manufacturer's instructions. RNA sample integrity was measured by Nanodrop spectrophotometry and Agilent Bioanalyzer. DNA sequencing libraries were prepared for sequencing on the Illumina GAIIx DNA sequencing instrument as follows: 1 μg of total RNA per sample was applied following the standard suggested methods outlined in the TruSeq RNA Library kit manual (Illumina). Following library generation, the resulting libraries were analyzed for quality by Bioanalyzer (Agilent) analysis to determine the appropriate size of the inserts, and concentration was ascertained by Qubit analysis (Life Technologies). Individual samples were diluted to 10 pM, each individual sample was placed within a single lane of the GAIIx instrument, and 75-base pairs paired-end sequencing was performed per the manufacturer's instructions. Sequences were mapped to the University of California at Santa Cruz hg19 reference genome using TopHat, along with Bowtie. The differential expression results were obtained by running Cufflinks, Cuffmerge, Cuffcompare, and Cuffdiff in order. Default parameters were used for all runs. The annotation was performed based on the RefSeq genes. Gene-expression and network-pathway analyses were conducted using Ingenuity pathway analysis (IPA). Selected potential genes (SPDEF, C13ORF15, SPP1, LIF, FGF19, MUC2, IGFBP5, MUTYH, DAPK1, and TNC) were validated by quantitative real-time PCR (qRT-PCR) using cDNA specific primers (*SI Appendix*, Table S10). Amplification of GAPDH was used to normalize the samples for comparison.

Kinetworks Multi-Immunoblotting Analysis. We analyzed phosphoproteins from T3M4 wild-type and *COSMC* KO cells Kinetworks multi-immunoblotting. Samples were prepared as recommended by Kinexus Bioinformatics (Kinexus Bioinformatics Corporation, Vancouver, B.C, Canada) for Kinetworks Phospho-Site Screen 1.3 (KPSS-1.3) analysis. The panel of target phosphoproteins detected by the KPSS-1.3 screens is listed on the Kinexus website.

In Vitro Migration and Invasion Analysis. In vitro migration and invasion analyses were performed in T3M4 wild-type, KO, and *COSMC* reexpression (CR) cells as described earlier (64). Briefly, tumor cells (0.25–0.5 × 10^6 cells) were seeded on top of the polyethylene terephthalate inserts and matrigel-coated Boyden chambers (BD Biosciences). Cells that transited the membrane were fixed and counted in five different fields (40× magnification) using a light microscope. The migratory status and invasiveness of the cells were expressed as the mean number of cells that migrated or invaded to the lower side of the membrane (triplicate wells). The experiments were repeated three times.

Organotypic Culture. Organotypic cultures were prepared as described (66). HaCaT cells and human fibroblasts were grown in Dulbecco's modified Eagle medium (DMEM) (Gibco, Life Technologies) supplemented with 10% (vol/vol) heat-inactivated FCS (HyClone), 100 IU/mL penicillin, and 100 μg/mL streptomycin (Gibco, Life Technologies). In brief, human abdominal skin fibroblasts suspended in 3 mL of rat-tail collagen I (4 mg/mL) were allowed to gel over a 1-mL layer of acellular collagen in six-well culture inserts with 3-μm–pore polycarbonate filters (BD Biosciences). Gels were allowed to contract for 4–5 d before seeding with 3 × 10^5 epithelial HaCaT cells in serum and mitogen-supplemented DMEM/F12 raft medium. Inserts were raised to the air–liquid interface 4 d later, and media were changed every second day for an additional 10 d. Four experiments conducted at different times with each cell line yielded organotypic cultures with similar morphologies.

Proliferation Assay. Cells were grown in 96-well culture plates in a volume of 200 μL of DMEM for 48 h. At the indicated time, the medium was discharged, and plates were rinsed in sterile PBS and frozen at −80 °C for at least 4 h. Cells were lysed, and the total cellular nucleic acid was measured using fluorescence at 520 nm emission after excitation at 480 nm using a CyQuant Cell Proliferation Assay Kit (Life Technologies) according to the manufacturer's protocol.

Scratch Assay. HaCaT wild-type and *COSMC* knockout cells were grown to confluence in DMEM with 10% FCS and antibiotics and washed with PBS. Several linear scratches were performed in each well, and subsequently the cells were grown for 72 h. Images of representative parts of the scratches were recorded immediately after scratching and after 24 h, 48 h, and 72 h with an Olympus LH50A microscope with a Leica DFC290 camera using Leica Application Suite v. 2.6.0 software (Leica Microsystems; www.leica-microsystems.com).

Dissociation Assay. HaCaT wild-type cells and *COSMC* knockout cells were grown to confluence and left confluent for 48 h in the incubator. For p38 inhibition, cells were treated with SB203580 (Enzo Life Sciences) for 24 h; for p38 activation, WT cells were treated with 80 μg/mL anisomycin (Sigma-Aldrich) for 24 h. To prevent anisomycin-induced p38 activation, cells were preincubated with SB203580 for 2 h. Cells were washed in HBSS (Gibco, Life Technologies) and incubated for 20 min in 2.4 mg/mL dispase II (Roche) in HBSS. Dispase was gently removed, the cells were pipetted up and down five times in a 1-mL pipet, and the number of fragments was counted.

Murine Tumor Models. ***Orthotopic pancreas tumor model.*** Implantation of tumor cells, tumor growth, and metastases was performed as described previously (67). Briefly, T3M4 wild-type, KO, and *COSMC* reexpression cells (0.25–0.5 × 10^6/30 μL PBS) were orthotopically implanted into the pancreas of athymic nu/nu mice (Crl:NU-Foxn1^{nu}) (n = 15 in each group). After 28 d, animals were killed, and the tumor weight, volume, and incidence of metastases were determined. All animal experiments were carried out according to protocols approved by the UNMC Institutional Animal Care and Use Committee. The statistical differences in tumor weight, volume, and metastasis were calculated by two-tailed Student t test and two-tailed Fisher's exact test.

Subcutaneous model. *COSMC* knockout HaCaT cells were inoculated s.c. into immune-deficient NOD.Cg- PrkdcscidB2mtm1Unc/J (NOD/SCID-B2m$^{-/-}$) mice (The Jackson Laboratory). This mouse strain is deficient for major histocompatibility complex class I B and T cells, as well as C-5, and has low natural killer cell activity. Tumor formation was detected on average 7 d after inoculation in 100% of the mice. After 31 d, the experiment was terminated, and tumor number and load in each group were determined. Tumors were dissected, fixed, sectioned, and stained for routine histology and immunocytochemistry. All animal experiments were carried out according to protocols approved by the Danish Animal Licence regulations (Forsøgsdyrstilsynet).

Antibodies. The following primary antibodies and dilutions were used: hybridoma supernatants against core 1 synthase (5F8), T antigen (HH8 and 3C9), Tn antigen (5F4), and STn antigen (TKH2 and 3F1). Antibodies against: Ki-67 (1:100; DAKO), cytokeratin 10 (1:50; DAKO), involucrin (1:100; Thermo Scientific), desmoglein-3 (1:50; R&D Systems), desmoglein-1 (R&D Systems), E-cadherin (1:800; R&D Systems), integrin-α3 (1:20; R&D Systems), integrin-α6 (1:100; R&D Systems), integrin-β4 (1:25; LS Biosciences), beta-catenin (1:800; DAKO), CD44 (1:1,000; R&D Systems), ZO-1 (1:200; BD Biosciences), p38 and phospho-p38 (1:1,000; both Cell Signaling Technologies), and Alexa Fluor 594 phalloidin (Molecular Probes, Life Technologies). The secondary antibodies used were Alexa Fluor 488 donkey anti-mouse IgG (H+L) or goat anti-rat IgG (H+L) or rabbit anti-mouse IgG (H+L) or 546 conjugated donkey anti-rabbit IgG (H+L) (Molecular Probes, Life Technologies) and FITC-conjugated goat anti-mouse IgG and IgM secondary antibody (Jackson ImmunoResearch).

Immunofluorescence. Standard immunofluorescence staining procedures were followed to stain the T3M4 wild-type, *COSMC* knockout (KO), and *COSMC* reexpressing (CR) cells with undiluted hybridoma supernatants of core 1 synthase (5F8), T antigen (HH8 and 3C9, 1:1 ratio, neuraminidase-treated), Tn antigen (5F4), and STn antigen (TKH2 and 3F1, 1:1 ratio) for 1 h at room temperature. Cells were washed and incubated with FITC-conjugated goat anti-mouse IgG and IgM secondary antibody (Jackson ImmunoResearch). Cells were washed and mounted with VECTASHIELD mounting medium with DAPI (Vector Laboratories). Cultured HaCaT WT and KO cells were grown on sterile coverslips (Thermo Scientific), fixed, and permeabilized in cold methanol/acetone (1:1), or fixed in fresh 4% paraformaldehyde and permeabilized with Triton X-100, and immunostained using the primary antibodies listed above with matching secondary Alexa Fluor antibodies (Molecular Probes). Organotypic cultures were fixed for 2 h at 4 °C in 10% neutral buffered formalin, paraffin-embedded, and cut as 2-μm sections for hematoxylin/eosin staining and immunostaining. Antigen retrieval was performed by microwaving slides submerged in either citrate buffer (pH 6) or Tris/EDTA buffer (pH 9) before staining sections for T/ST/Tn/STn antigens and Ki-67. Sections were permeabilized using 0.3% Triton X-100 (Sigma-Aldrich) before staining for desmoglein-3. Sections or coverslips were mounted with ProLong Gold Antifade Reagent with DAPI (Life Technologies).

Frozen tissue specimens of *COSMC*-methylated (n = 9) and -nonmethylated (n = 9) tumor samples were sectioned (4–7 μm) and fixed in 10% neutral buffered formalin for 10–15 min. Sections were blocked with Protein Block (Dako) and incubated with undiluted hybridoma supernatants specific for core 1 synthase (5F8), T [HH8 and 3C9, 1:1 ratio (tissues were briefly treated with neuraminidase before antibody incubation); Sigma-Aldrich], Tn (1E3 and 5F4, 1:1 ratio), and sialyl Tn antigen (3F1, TKH2, and B72.3, 1:1:1 ratio). Slides were incubated overnight and labeled with Alexa Fluor 6470-conjugated goat anti-mouse IgG and IgM (Molecular Probes, Life Technologies) and mounted with DAPI containing mounting medium (VECTASHIELD; Vector Laboratories). The positive staining of tumor and stromal cells was scored (0 = negative, 1 = 0–25%, 2 = 25–50%, 3 = 50–75%, 4 = 75–100%) and plotted as a heat map. All immunofluorescence images on cultured cells and tissue sections were captured on a Zeiss LSM 710 confocal microscope.

Transmission Electron Microscopy. Samples were fixed with 2% (vol/vol) glutaraldehyde in 0.05 M sodium phosphate buffer (pH 7.2), rinsed three times in 0.15 M sodium cacodylate buffer (pH 7.2), and subsequently post-fixed in 1% (wt/vol) OsO_4 in 0.12 M sodium cacodylate buffer (pH 7.2) for 2 h. The specimens were dehydrated in a graded series of ethanol, transferred to propylene oxide, and embedded in Epon according to standard procedures. Sections, ∼80 nm thick, were cut with a Reichert-Jung Ultracut E microtome and collected on one-hole copper grids with Formvar supporting membranes, stained with uranyl acetate and lead citrate, and subsequently examined with a Philips CM 100 TEM (Philips, Eindhoven), operated at an accelerating voltage of 80 kV and equipped with an OSIS Veleta digital slow scan 2,000 × 2,000 CCD camera. Digital images were recorded with the ITEM software package.

Western Blotting. Proliferating cultures were trypsinized, PBS-rinsed, and lysed in 20 mM Tris buffer (pH 7.3), with 2% SDS protease inhibitor mixture (Roche Diagnostics; www.roche-appliedscience.com). Then, 5–10 μg (Bio-Rad assay) of extract protein was separated by SDS/PAGE under reducing conditions in precast, 4–20% gradient gels (Bio-Rad; www.bio-rad.com) and electrotransferred to PVDF membranes (Millipore), and specific proteins were detected by incubation with primary antibodies, peroxidase-conjugated secondary antibody (Southern Biotech), and ECL chemiluminescence reagent (Amersham; www.amersham.com).

O-Glycoproteome Analysis. Sample preparation and lectin enrichment were performed as previously described (31, 32) and as described in detail in *SI Appendix*. All glycoprotein analysis was performed on HaCaT KO#1. In short, conditioned media were cleared by centrifugation, dialyzed, and neuraminidase-treated, and glycoproteins were enriched by capture on a short VVA agarose column. Glycoproteins were eluted, dialyzed, and concentrated. Total cell lysates (TCL) were obtained by addition of RapiGest to cell pellets. TCLs and glycoprotein-enriched media were reduced, alkylated, and digested by either trypsin, chymotrypsin, GluC, or Asp-N. The digests were subsequently loaded on a 2.6-m-long VVA agarose column, eluted with GalNAc, and submitted for MS analysis (XL). The most complex fractions were pooled and fractionated further by isoelectric focusing (IEF) and analyzed on an EASY-nLC II interfaced via nanoSpray Flex ion source to an LTQ-Orbitrap XL ETD spectrometer (Thermo Fisher Scientific). All MS1, HCD-MS2, and ETD-MS2 spectra were acquired in the Orbitrap sector; MS data analysis was performed using Proteome Discoverer 1.2 software, assisted by manual validation (31, 32). The results obtained were accumulated in a single list (*SI Appendix*, Table S4).

Phosphoproteome Profiling of Wild-Type and *COSMC* Knockout HaCaT Cells. HaCaT cells were grown as described in *Organotypic Culture*. Media and reagents specifically designed for analysis of protein by mass spectrometry (Thermo Scientific) were used for stable isotope labeling by amino acids in cell culture (SILAC) experiments. Phosphopeptide enrichment, mass spectrometric analysis, MS data analysis (including peptide filtering and phosphorylation site localization), and phosphorylation site sequence motif logo plots were done as previously described (34, 68) and as described in detail in *SI Appendix*.

ACKNOWLEDGMENTS. This work was in part supported by the Danish Research Councils (Sapere Aude), Programme of Excellence 2016 Grant CDO2016 from the University of Copenhagen, The Lundbeck Foundation, A.P. Møller og Hustru Chastine Mc-Kinney Møllers Fond til Almene Formaal, Kirsten og Freddy Johansen Fonden, the Carlsberg Foundation, the Novo Nordisk Foundation, Danish National Research Foundation Grant DNRF107, Early Detection Research Network Grant 5U01CA111294, Alliance of Glycobiologists for Detection of Cancer and Cancer Risk Grant 5U01CA128437, National Institutes of Health (NIH) Specialized Program of Research Excellence Grant 5P50CA127297, and NIH Grant R01CA57362. C.F. is supported by a Marie Curie Intra-European Fellowship and a European Molecular Biology Organization long-term fellowship.

1. Hakomori S (2001) Tumor-associated carbohydrate antigens defining tumor malignancy: Basis for development of anti-cancer vaccines. *Adv Exp Med Biol* 491:369–402.
2. Springer GFT (1984) T and Tn, general carcinoma autoantigens. *Science* 224(4654): 1198–1206.
3. Itzkowitz S, et al. (1991) Expression of Tn, sialosyl Tn, and T antigens in human pancreas. *Gastroenterology* 100(6):1691–1700.
4. Tarp MA, Clausen H (2008) Mucin-type O-glycosylation and its potential use in drug and vaccine development. *Biochim Biophys Acta* 1780(3):546–563.
5. Ching CK, Holmes SW, Holmes GK, Long RG (1993) Comparison of two sialosyl-Tn binding monoclonal antibodies (MLS102 and B72.3) in detecting pancreatic cancer. *Gut* 34(12):1722–1725.
6. Lyubsky S, et al. (1988) A tumor-associated antigen in carcinoma of the pancreas defined by monoclonal antibody B72.3. *Am J Clin Pathol* 89(2):160–167.
7. Kim GE, et al. (2002) Aberrant expression of MUC5AC and MUC6 gastric mucins and sialyl Tn antigen in intraepithelial neoplasms of the pancreas. *Gastroenterology* 123(4):1052–1060.
8. Springer GF (1997) Immunoreactive T and Tn epitopes in cancer diagnosis, prognosis, and immunotherapy. *J Mol Med (Berl)* 75(8):594–602.
9. Schietinger A, et al. (2006) A mutant chaperone converts a wild-type protein into a tumor-specific antigen. *Science* 314(5797):304–308.
10. Wandall HH, et al. (2010) Cancer biomarkers defined by autoantibody signatures to aberrant O-glycopeptide epitopes. *Cancer Res* 70(4):1306–1313.
11. Ju T, et al. (2013) Tn and sialyl-Tn antigens, aberrant O-glycomics as human disease markers. *Proteomics Clin Appl*, 10.1002/prca.201300024.
12. Stanley P (2011) Golgi glycosylation. *Cold Spring Harb Perspect Biol* 3(4):a005199.
13. Ju T, Aryal RP, Stowell CJ, Cummings RD (2008) Regulation of protein O-glycosylation by the endoplasmic reticulum-localized molecular chaperone Cosmc. *J Cell Biol* 182(3): 531–542.
14. Ju T, Cummings RD (2002) A unique molecular chaperone Cosmc required for activity of the mammalian core 1 beta 3-galactosyltransferase. *Proc Natl Acad Sci USA* 99(26): 16613–16618.
15. Ju T, et al. (2008) Human tumor antigens Tn and sialyl Tn arise from mutations in Cosmc. *Cancer Res* 68(6):1636–1646.
16. Wang Y, et al. (2010) Cosmc is an essential chaperone for correct protein O-glycosylation. *Proc Natl Acad Sci USA* 107(20):9228–9233.
17. Sewell R, et al. (2006) The ST6GalNAc-I sialyltransferase localizes throughout the Golgi and is responsible for the synthesis of the tumor-associated sialyl-Tn O-glycan in human breast cancer. *J Biol Chem* 281(6):3586–3594.
18. Ju T, Cummings RD (2005) Protein glycosylation: Chaperone mutation in Tn syndrome. *Nature* 437(7063):1252.
19. Gill DJ, et al. (2013) Initiation of GalNAc-type O-glycosylation in the endoplasmic reticulum promotes cancer cell invasiveness. *Proc Natl Acad Sci USA* 110(34): E3152–E3161.
20. Gill DJ, Chia J, Senewiratne J, Bard F (2010) Regulation of O-glycosylation through Golgi-to-ER relocation of initiation enzymes. *J Cell Biol* 189(5):843–858.
21. Marcos NT, et al. (2004) Role of the human ST6GalNAc-I and ST6GalNAc-II in the synthesis of the cancer-associated sialyl-Tn antigen. *Cancer Res* 64(19):7050–7057.
22. Axelsson MA, et al. (2001) Neutralization of pH in the Golgi apparatus causes redistribution of glycosyltransferases and changes in the O-glycosylation of mucins. *Glycobiology* 11(8):633–644.
23. Hassinen A, et al. (2011) Functional organization of Golgi N- and O-glycosylation pathways involves pH-dependent complex formation that is impaired in cancer cells. *J Biol Chem* 286(44):38329–38340.
24. Remmers N, et al. (2013) Aberrant expression of mucin core proteins and o-linked glycans associated with progression of pancreatic cancer. *Clin Cancer Res* 19(8): 1981–93.
25. Pellegata NS, et al. (1994) K-ras and p53 gene mutations in pancreatic cancer: Ductal and nonductal tumors progress through different genetic lesions. *Cancer Res* 54(6): 1556–1560.
26. Mi R, et al. (2012) Epigenetic silencing of the chaperone Cosmc in human leukocytes expressing tn antigen. *J Biol Chem* 287(49):41523–41533.
27. Steentoft C, et al. (2011) Mining the O-glycoproteome using zinc-finger nuclease-glycoengineered SimpleCell lines. *Nat Methods* 8(11):977–982.
28. Boukamp P, et al. (1988) Normal keratinization in a spontaneously immortalized aneuploid human keratinocyte cell line. *J Cell Biol* 106(3):761–771.
29. Boukamp P, et al. (1997) Sustained nontumorigenic phenotype correlates with a largely stable chromosome content during long-term culture of the human keratinocyte line HaCaT. *Genes Chromosomes Cancer* 19(4):201–214.
30. Beck B, Blanpain C (2012) Mechanisms regulating epidermal stem cells. *EMBO J* 31(9): 2067–2075.
31. Vakhrushev SY, et al. (2013) Enhanced mass spectrometric mapping of the human GalNAc-type O-glycoproteome with SimpleCells. *Mol Cell Proteomics* 12(4):932–944.
32. Steentoft C, et al. (2013) Precision mapping of the human O-GalNAc glycoproteome through SimpleCell technology. *EMBO J* 32(10):1478–1488.
33. Ponta H, Sherman L, Herrlich PA (2003) CD44: From adhesion molecules to signalling regulators. *Nat Rev Mol Cell Biol* 4(1):33–45.
34. Olsen JV, et al. (2006) Global, in vivo, and site-specific phosphorylation dynamics in signaling networks. *Cell* 127(3):635–648.
35. Rigbolt KT, et al. (2011) System-wide temporal characterization of the proteome and phosphoproteome of human embryonic stem cell differentiation. *Sci Signal* 4(164):rs3.
36. Kelstrup CD, Hekmat O, Francavilla C, Olsen JV (2011) Pinpointing phosphorylation sites: Quantitative filtering and a novel site-specific x-ion fragment. *J Proteome Res* 10(7):2937–2948.
37. Spindler V, et al. (2013) Peptide-mediated desmoglein 3 crosslinking prevents pemphigus vulgaris autoantibody-induced skin blistering. *J Clin Invest* 123(2):800–811.
38. Hruban RH, Goggins M, Parsons J, Kern SE (2006) Progression model for pancreatic cancer. *Clin Cancer Res* 6(8):2969–2972.
39. Boukamp P, Stanbridge EJ, Foo DY, Cerutti PA, Fusenig NE (1990) c-Ha-ras oncogene expression in immortalized human keratinocytes (HaCaT) alters growth potential in vivo but lacks correlation with malignancy. *Cancer Res* 50(9):2840–2847.
40. Breitkreutz D, et al. (1991) Epidermal morphogenesis and keratin expression in c-Ha-ras-transfected tumorigenic clones of the human HaCaT cell line. *Cancer Res* 51(16): 4402–4409.
41. Boukamp P, et al. (1999) Tumorigenic conversion of immortal human skin keratinocytes (HaCaT) by elevated temperature. *Oncogene* 18(41):5638–5645.
42. Breitkreutz D, et al. (1998) Epidermal differentiation and basement membrane formation by HaCaT cells in surface transplants. *Eur J Cell Biol* 75(3):273–286.
43. Breitkreutz D, Stark HJ, Plein P, Baur M, Fusenig NE (1993) Differential modulation of epidermal keratinization in immortalized (HaCaT) and tumorigenic human skin keratinocytes (HaCaT-ras) by retinoic acid and extracellular Ca2+. *Differentiation* 54(3): 201–17.
44. Lederle W, Stark HJ, Skobe M, Fusenig NE, Mueller MM (2006) Platelet-derived growth factor-BB controls epithelial tumor phenotype by differential growth factor regulation in stromal cells. *Am J Pathol* 169(5):1767–1783.
45. Skobe M, Fusenig NE (1998) Tumorigenic conversion of immortal human keratinocytes through stromal cell activation. *Proc Natl Acad Sci USA* 95(3):1050–1055.
46. Lederle W, et al. (2011) IL-6 promotes malignant growth of skin SCCs by regulating a network of autocrine and paracrine cytokines. *Int J Cancer* 128(12):2803–14.
47. Mueller MM, Fusenig NE (1999) Constitutive expression of G-CSF and GM-CSF in human skin carcinoma cells with functional consequence for tumor progression. *Int J Cancer* 83(6):780–9.
48. Obermueller E, Vosseler S, Fusenig NE, Mueller MM (2004) Cooperative autocrine and paracrine functions of granulocyte colony-stimulating factor and granulocyte-macrophage colony-stimulating factor in the progression of skin carcinoma cells. *Cancer Res* 64(21):7801–7812.
49. Margulis A, et al. (2003) Abrogation of E-cadherin-mediated adhesion induces tumor cell invasion in human skin-like organotypic culture. *J Invest Dermatol* 121(5): 1182–1190.
50. Margulis A, et al. (2005) E-cadherin suppression accelerates squamous cell carcinoma progression in three-dimensional, human tissue constructs. *Cancer Res* 65(5):1783–1791.
51. Bennett EP, et al. (2012) Control of mucin-type O-glycosylation: A classification of the polypeptide GalNAc-transferase gene family. *Glycobiology* 22(6):736–756.
52. Sørensen AL, Clausen H, Wandall HH (2012) Carbohydrate clearance receptors in transfusion medicine. *Biochim Biophys Acta* 1820(11):1797–1808.
53. Schjoldager KT, Clausen H (2012) Site-specific protein O-glycosylation modulates proprotein processing: Deciphering specific functions of the large polypeptide GalNAc-transferase gene family. *Biochim Biophys Acta* 1820(12):2079–2094.
54. Ohtsubo K, Marth JD (2006) Glycosylation in cellular mechanisms of health and disease. *Cell* 126(5):855–867.
55. Moremen KW, Tiemeyer M, Nairn AV (2012) Vertebrate protein glycosylation: Diversity, synthesis and function. *Nat Rev Mol Cell Biol* 13(7):448–462.
56. Maxson JE, et al. (2014) Ligand independence of the T618I mutation in the colony-stimulating factor 3 receptor (CSF3R) protein results from loss of O-linked glycosylation and increased receptor dimerization. *J Biol Chem* 289(9):5820–5827.
57. Harmon RM, et al. (2013) Desmoglein-1/Erbin interaction suppresses ERK activation to support epidermal differentiation. *J Clin Invest* 123(4):1556–1570.
58. Lavrsen K, et al. (2013) Aberrantly glycosylated MUC1 is expressed on the surface of breast cancer cells and a target for antibody-dependent cell-mediated cytotoxicity. *Glycoconj J* 30(3):227–236.
59. DePristo MA, et al. (2011) A framework for variation discovery and genotyping using next-generation DNA sequencing data. *Nat Genet* 43(5):491–498.
60. Koboldt DC, et al. (2012) VarScan 2: Somatic mutation and copy number alteration discovery in cancer by exome sequencing. *Genome Res* 22(3):568–576.
61. McKenna A, et al. (2010) The Genome Analysis Toolkit: A MapReduce framework for analyzing next-generation DNA sequencing data. *Genome Res* 20(9):1297–1303.
62. Hlady RA, et al. (2012) Loss of Dnmt3b function upregulates the tumor modifier Ment and accelerates mouse lymphomagenesis. *J Clin Invest* 122(1):163–177.
63. Li LC, Dahiya R (2002) MethPrimer: Designing primers for methylation PCRs. *Bioinformatics* 18(11):1427–1431.
64. Radhakrishnan P, et al. (2013) Expression of core 3 synthase in human pancreatic cancer cells suppresses tumor growth and metastasis. *Int J Cancer* 133(2):2824–33.
65. Breitling R, Armengaud P, Amtmann A, Herzyk P (2004) Rank products: A simple, yet powerful, new method to detect differentially regulated genes in replicated microarray experiments. *FEBS Lett* 573(1-3):83–92.
66. Dabelsteen S, et al. (2009) Epithelial cells derived from human embryonic stem cells display p16INK4A senescence, hypermotility, and differentiation properties shared by many P63+ somatic cell types. *Stem Cells* 27(6):1388–1399.
67. Burdick MD, Harris A, Reid CJ, Iwamura T, Hollingsworth MA (1997) Oligosaccharides expressed on MUC1 produced by pancreatic and colon tumor cell lines. *J Biol Chem* 272:24198–24202.
68. Olsen JV, et al. (2007) Higher-energy C-trap dissociation for peptide modification analysis. *Nat Methods* 4(9):709–712.